



Cite this: DOI: 10.1039/d3ja00162h

Characterization of reference materials for *in situ* U–Pb dating of columbite group minerals by LA-ICP-MS†

 Ming Yang,^{a,b} Yue-Heng Yang,^b Rolf L. Romer,^c Xu-Dong Che,^d Ru-Cheng Wang,^d Fu-Yuan Wu,^b Guang-Chun Fei,^f Yun Deng^f and Tao Wu^{ae}

Columbite group minerals generally incorporate considerable amounts of U, making them promising minerals for *in situ* U–Pb dating and constraining the time of Nb–Ta mineralization. Columbite group minerals may have uranium-rich inclusions and metamict domains and may show complex internal textures with recrystallization. To avoid such disturbances, isotopic measurements with high spatial resolution are needed. The laser ablation inductively coupled plasma mass spectrometry (LA-ICP-MS) technique, which is widely used for U–Pb dating with high spatial resolution, requires homogeneous reference materials for external calibration. Herein, we present *in situ* U–Pb ages, ranging from ~2050 Ma to ~136 Ma and chemical compositions for ten columbite group minerals considered potential reference materials. Our study indicates that CT3, Buranga, Rongi and SN3 contain very limited amounts of common Pb and can be used as primary reference materials for *in situ* U–Pb dating. Coltan17, ZKW, DDB, HND and RL2 show variable common Pb contents but have robust U–Pb ages that allow them to be used as primary reference materials. Among them, Coltan17 needs to be further characterized by applying the isotope dissolution thermal ionization mass spectrometry (ID-TIMS) method. A new ID-TIMS weighted average ²⁰⁶Pb/²³⁸U age of Coltan139 of 507.8 ± 1.3 Ma (2s, MSWD = 0.9; n = 6) is reported. This study demonstrates that Coltan139 contains relatively high and variable common Pb contents. Therefore, special attention should be given to the selected measurement areas when using Coltan139 as the primary reference material.

Received 19th May 2023

Accepted 11th July 2023

DOI: 10.1039/d3ja00162h

rsc.li/jaas

1 Introduction

Niobium and tantalum are economically important resources owing to their wide application in emerging high-tech fields. Columbite group minerals (CGMs) are the most important niobium- and tantalum-bearing economic minerals that mainly occur in rare metal granites, pegmatites and hydrothermal veins,^{1–3} which have been used as U–Pb geochronometers owing to their high U contents and low common Pb contents.^{4–7} Dating columbite group minerals provides a direct step in connecting

the formation of Nb and Ta resources to the magmatic and tectonic history of the area. Most importantly, CGM U–Pb dating can yield the emplacement age of rocks, such as highly evolved rare element granites and pegmatites, which typically are hard to date using the more commonly used minerals zircon and monazite.^{8,9} The age of CGM can also be used to fingerprint the provenance of columbite–tantalite minerals to provide transparency along trade chains.^{10–12}

The first results of U–Pb dating of columbite–tantalite minerals using isotope-dilution thermal ionization mass spectrometry (ID-TIMS) were published by Aldrich *et al.*¹³ They obtained a discordant U–Pb age for a columbite–tantalite sample from the Brown Derby pegmatite. CGM may have abundant uranium-rich inclusions, metamict zones, and complex internal textures reflecting recrystallization.^{5,14–18} Romer and Wright⁴ chemically removed inclusions and altered domains selectively during CGM sample preparation and illustrated that the U–Pb dating of columbite group minerals is a potentially powerful tool to constrain the age of columbite-bearing granites, pegmatites, and alkaline and carbonatitic intrusions. Even though high precision ID-TIMS U–Pb dating of CGM involves a tedious and time-consuming chemical separation procedure and has limited spatial resolution, the setup was increasingly

^aHainan Institute of Zhejiang University, Sanya, Hainan Province, 572025, P. R. China

^bState Key Laboratory of Lithospheric Evolution, Institute of Geology and Geophysics, Chinese Academy of Sciences, Beijing, 100029, P. R. China. E-mail: yangyueheng@mail.iggcas.ac.cn

^cGFZ German Research Centre for Geosciences, Telegrafenberg, Potsdam, 14473, Germany

^dState Key Laboratory for Mineral Deposits Research, School of Earth Sciences and Engineering, Nanjing University, Xianlin University Town, Nanjing 210023, China

^eOcean College, Zhejiang University, Zhoushan, Zhejiang Province, 316021, P. R. China

^fCollege of Earth Science, Chengdu University of Technology, Chengdu, Sichuan Province, 610059, P. R. China

 † Electronic supplementary information (ESI) available. See DOI: <https://doi.org/10.1039/d3ja00162h>

used because of an increased interest in rare metal pegmatites.^{1,5,6,14–22} The time-consuming procedure, the limited spatial resolution, and the large sample consumption^{23,24} resulted in an increasingly more important substitution of ID-TIMS U–Pb dating of CGM by *in situ* U–Pb age determinations. The latter requires reliable reference material.

Smith *et al.*⁷ first reported *in situ* CGM U–Pb ages using laser ablation multi-collector inductively coupled plasma mass spectrometry (LA-MC-ICP-MS). Moreover, CGM has been dated using other *in situ* techniques, such as secondary ionization mass spectrometry (SIMS),²⁵ and most importantly LA-ICP-MS.^{9,11,26–32} The major limitation of *in situ* U–Pb dating is the absence of matrix-matched materials with well-characterized U–Pb systematics. Some early studies used non-matrix-matched monazite and zircon as external calibration standards and observed large variations in the obtained results. Smith *et al.*⁷ used monazite as an external calibration standard and documented up to 20% matrix-dependent fractionation for the ²³⁸U/²⁰⁶Pb ratio. Che *et al.*²⁹ used zircon as an external calibration standard and obtained up to 11% matrix-dependent fractionation for the ²³⁸U/²⁰⁶Pb ratio. The matrix-mismatched reference materials showed contrasting fractionation to CGM samples.²⁹ Other studies have not observed matrix-dependent U/Pb fractionation for *in situ* CGM U–Pb dating.^{26,31,33} Thus, favourable analytical settings (such as the wavelength of the laser ablation system, energy density, and laser spot size)³⁴ may minimize the effect of a non-matching matrix. However, matrix-matched secondary reference material is needed for quality control of the analytical data.

There are only a few established CGM reference materials available for *in situ* U–Pb dating. Among these samples, Coltan139 is the most commonly used CGM reference material. Gäbler *et al.*¹⁰ first used this sample as an in-house reference material. Later, Coltan139 was characterized by Che *et al.*²⁹ This sample had been dated by ID-TIMS¹¹ although the analytical data were not reported. Recently, Legros *et al.*²⁵ and Xiang *et al.*³⁴ introduced several reference materials for *in situ* CGM U–Pb dating. However, these newly developed reference materials have not been widely distributed and need to be further examined for their elemental and isotopic homogeneity.

The main objectives of this study are as follows: (i) examine the elemental and isotopic homogeneity of the CGM samples investigated in this study; (ii) re-evaluate the feasibility of Coltan139 as a reference material; and (iii) develop new CGM reference materials suitable for *in situ* U–Pb dating.

2 Materials and methods

2.1 Sample description

2.1.1 CT1 and CT3. CT1 and CT3 were collected from placers in the central-west Ivory Coast. The placers are directly related to local granites and pegmatites. These two samples were dated by both ID-TIMS and SIMS techniques by Legros *et al.*²⁵ and obtained ID-TIMS ²⁰⁷Pb/²⁰⁶Pb ages of 2046.8 ± 1.1 Ma (2s, MSWD = 2.2) and 2053.2 ± 1.3 Ma (2s, MSWD = 2.2), respectively.

2.1.2 Rongi and Buranga, Rwanda. The Rongi and Buranga samples were collected from the pegmatites of the Karagwe-Ankole belt of Central Africa. These two samples were dated by applying the ID-TIMS method. Dewaele *et al.*²⁷ and Melcher *et al.*¹¹ reported concordia ages of 936 ± 14 Ma (2s, MSWD = 2.5) and 931.1 ± 1.2 Ma (2s, MSWD = 2.0), respectively, for Rongi. Legros *et al.*²⁵ reported ID-TIMS concordia ages of 931.5 ± 2.5 Ma (2s, MSWD = 0.8) for Rongi and 905.2 ± 3.2 Ma (2s, MSWD = 0.4) for Buranga. A SIMS U–Pb age of 905.0 ± 5.0 Ma (2s, MSWD = 0.9) for Rongi was also reported by Legros *et al.*²⁵ Sample Rongi may be homogeneous on a mineral scale but heterogeneous between different crystals. The younger age of the Buranga sample may reflect the presence of several generations of pegmatites in the region or that some pegmatites have been overprinted, leading to the formation of several generations of columbite. The Buranga sample investigated here was obtained from Legros *et al.*²⁵

2.1.3 Coltan139, Madagascar. Coltan139 was first investigated by Gäbler *et al.*¹⁰ and used as an in-house reference material for CGM U–Pb dating. Melcher *et al.*¹¹ reported two ID-TIMS ages of 505.4 ± 1.0 Ma (2s, MSWD = 2.7; Bundesanstalt für Geowissenschaften und Rohstoffe (BGR), Hannover, Germany) and 506.6 ± 2.4 Ma (2s, MSWD = 0.23; University of Toronto), and a LA-ICP-MS age of 506.2 ± 5.0 Ma (2s, MSWD = 0.93; University of Frankfurt). Che *et al.*²⁹ further characterized Coltan139 and used it as primary reference material for *in situ* CGM U–Pb dating.

2.1.4 Coltan17, Brazil. Coltan17 is a CGM sample from Brazil. Geological background information is absent. Gäbler *et al.*¹⁰ presented a U–Pb LA-ICP-MS age of ~502 Ma for Coltan17. Yuan *et al.*³² used Coltan17 for quality control during *in situ* columbite–tantalite U–Pb dating and reported a U–Pb age of 502.8 ± 7.5 Ma (2s, MSWD = 0.03).

2.1.5 SN3, Shanxi Province, China. SN3 was collected from the Shangnan Li–Be–Cs–Nb–Ta pegmatite district located in the eastern part of the Qinling Orogen in Shangnan County, Shanxi Province, China.³⁵ There are two episodes of pegmatitic emplacement at 399–363 Ma and 422–410 Ma.^{25,29,33,36} Xiang *et al.*³⁴ reported an ID-TIMS age of 404.0 ± 1.3 Ma (2s, MSWD = 2.2).

2.1.6 ZKW and DDB, Sichuan Province, China. Samples ZKW and DDB were both collected from the newly discovered Ke'eryin ore field in west Sichuan Province, China. This ore field in the central Songpan-Garze fold belt (SGFB) hosts pegmatite-type lithium deposits with niobium, tantalum, beryllium, rubidium and tin.³⁷ Sample ZKW was collected from the Lijiagou spodumene pegmatite. Fei *et al.*³⁷ reported zircon, cassiterite and columbite–tantalite LA-ICP-MS U–Pb ages of 200.1 ± 4.6 Ma, 211.4 ± 3.3 Ma and 211.1 ± 1.0 Ma for albite spodumene pegmatites. Sample DDB was collected from the Dangba granitic pegmatite type rare-metal deposit. LA-ICP-MS cassiterite U–Pb dating of two cassiterite samples from this deposit gives ages of 208.1 ± 1.9 Ma (2s, MSWD = 2.5) and 199.3 ± 1.6 Ma (2s, MSWD = 0.7).³⁸

2.1.7 HND and RL2, the junction of Hunan and Hubei Province, China. HND and RL2 samples were introduced by

Xiang *et al.*³⁴ and collected from two pegmatite districts located in the eastern part of the Jiangnan Orogen at the boundary between the Hunan and Hubei provinces, China. Earlier studies showed that the pegmatite dykes of this area were mainly intruded at 133–140 Ma.³⁹ Xiang *et al.*³⁴ reported ID-TIMS U–Pb ages of 136.2 ± 0.9 Ma (2s, MSWD = 2.4) and 135.7 ± 0.3 Ma (2s, MSWD = 0.6) for the HND and RL2 samples, respectively.

2.2 Instrumentation

2.2.1 Electron microprobe analysis (EPMA). Quantitative major element analysis of CGM samples was performed using a CAMECA SX Five Electron Microprobe housed at the Electron Microprobe and Scanning Electron Microscope Laboratory, Institute of Geology and Geophysics, Chinese Academy of Sciences, Beijing, China. The operating conditions included a beam current of 3×10^{-8} A with 15 kV acceleration voltage and 5 μm beam diameter. The peak counting time was 20 s for all elements, and the background counting time was 10 s for the high- and low-energy background positions. Natural minerals (scheelite), compounds (SnO_2 and MnTiO_3), and pure metals (Nb, Ta, and Sc) were used as standards. The detection limit is better than 0.1% m/m for the analyzed elements.

2.2.2 *In situ* trace elements and U–Pb determination. The trace elements and U–Pb dating analyses were conducted at the Institute of Geology and Geophysics, Chinese Academy of Sciences, using an Agilent 7500a Q-ICP-MS coupled to a Geolas HD (Coherent, USA) 193 nm nanosecond laser ablation system with a pulse width of 4 ns. The NIST SRM 610 standard glass⁴⁰ was used to optimize the instrument during laser ablation. Helium was used as the carrier gas and mixed with argon before entering the ICP torch. The parameters of the two gases were optimized to obtain a stable maximum signal intensity for

$^{238}\text{U}^+$, while suppressing oxide formation and limiting fractionation between U and Th, using the ThO^+/Th^+ (<0.5%) and Th/U ratios (approximately 1) as monitors. Detailed parameter settings are presented in Table 1. The laser was operated at ~ 5 J cm^{-2} fluence, 32 μm spot size and 5 Hz repetition rate. All LA-ICP-MS measurements were carried out using time-resolved analysis in fast peak jumping mode. The measurement time for each isotope was set at 6 ms for Sc, Zn, Y, Zr, Hf and REE; 10 ms for ^{232}Th and ^{238}U ; 15 ms for ^{204}Pb , ^{206}Pb , and ^{208}Pb ; and 30 ms for ^{207}Pb . Each spot analysis includes ~ 15 s background, ~ 15 s washout and 60 s data acquisition.^{41,42} A matrix matched CGM reference material (CT1)²⁵ was used as the primary standard to correct $^{207}\text{Pb}/^{206}\text{Pb}$, $^{206}\text{Pb}/^{238}\text{U}$, $^{207}\text{Pb}/^{235}\text{U}$ (using $^{238}\text{U}/^{235}\text{U} = 137.818$)⁴³ and $^{208}\text{Pb}/^{232}\text{Th}$ ratios. Coltan139 (ref. 29) and SN3 (ref. 34) were used as secondary reference materials to monitor data reproducibility. The NIST SRM 610 glass⁴⁰ was used as the primary reference material, and ARM-1 synthetic glass⁴⁴ was used for quality control of trace element analysis. Trace element concentrations were calibrated using ^{55}Mn as the internal standard (MnO contents were measured by EPMA). Isotopic and elemental fractionation along with instrumental mass bias were calibrated using Glitter 4.0 software.⁴⁵ All signal intervals of the standards and unknown samples were selected independently to obtain similar signal sections. The ^{204}Pb correction was not used owing to considerable amounts of tungsten in columbite–tantalite minerals (it may form $^{186}\text{W}^{16}\text{O}^+$)^{23,46} and minor $^{204}\text{Hg}^+$, which might affect the measurement of $^{204}\text{Pb}^+$. The ^{207}Pb correction slightly affects the obtained U–Pb ages²³ and has been employed for samples with common Pb. For samples with variable common Pb contents, all data are plotted on Tera–Wasserburg diagrams and presented as discordias forced through $^{207}\text{Pb}/^{206}\text{Pb}$ ratios estimated using the Stacey and Kramers⁴⁸ crustal Pb model and the

Table 1 Typical instrument parameters for U–Pb dating and trace element analysis of CGM samples by LA-ICP-MS

Laser ablation system	Coherent Geolas HD
Laser ablation system	ComPex 102, ArF excimer UV 193 nm
Ablation cell and volume	Standard circle low volume cell Volume <i>ca.</i> 4 cm^3
Fluence	~ 5 J cm^{-2} for trace element analysis and U–Pb dating
Repetition rate	5 Hz
Spot diameter nominal	32 μm for trace elements analysis and U–Pb dating
Ablation duration	60 s for trace elements and U–Pb dating
Sampling mode	Static spot ablation
Sample preparation	Conventional mineral separation, 1-inch resin mount
Mass spectrometer	Agilent 7500a Q-ICP-MS
RF forward power (W)	~ 1350
Carrier gas (L min^{-1})	~ 1.1
Cool gas (L min^{-1})	~ 14
Sample depth (mm)	~ 4.5
Interface cone	Ni
Isotopes detected and dwell time	15 ms for ^{204}Pb , ^{206}Pb and ^{208}Pb , 30 ms for ^{207}Pb , 10 ms for ^{232}Th and ^{238}U , 6 ms for isotopes of other elements
Analysis duration	90 s (including 30 s background) 60 s ablation

age of the sample. Isoplot 4.15 (ref. 47) was used to make plots and age calculations.

2.2.3 U–Pb ID-TIMS dating. U–Pb dating of the CGM by ID-TIMS was completed at the GFZ German Research Centre for Geosciences, Potsdam, essentially using the analytical procedure described in Romer and Smeds.¹⁵ To avoid contributions from common Pb-bearing inclusions (silicate and sulphide minerals) and metamict domains (high U contents), which may behave as open systems, all analysed fragments were treated with 20% HF, 6 mol L⁻¹ HCl and 7 mol L⁻¹ HNO₃ for 20 minutes each on a ~70 °C hotplate. This procedure resulted in the preferred removal of silicate and sulphide minerals, and the dissolution of sections strongly damaged by α -recoil¹⁴ and may cause the U and Pb contents of the ID-TIMS analyses to be lower than for *in situ* analysis. After the pretreatment, all samples were rinsed in H₂O and acetone.

After the addition of a mixed ²⁰⁵Pb–²³⁵U tracer and a small amount of H₂SO₄, the columbite group minerals were dissolved in 40% HF on a 160 °C hot plate overnight. Uranium and Pb were separated using ion exchange chemistry, as described in Romer and Smeds.¹⁵ Uranium and Pb were loaded with H₃PO₄ and silica gel on separate Re single filaments. The isotopic ratios of U and Pb were measured using a Triton TIMS operated in static or dynamic multi-collection mode, depending on signal intensity, using Faraday collectors and an ion counter. Lead was analyzed at 1200–1260 °C and U at 1380–1450 °C. Data were corrected for 15 pg Pb blank, 1 pg U blank and tracer contribution. Common Pb was corrected based on the measured ²⁰⁴Pb content and the Pb evolution model of Stacey and Kramers.⁴⁸ The analytical results are presented in Table 3. The precision for Pb–U and Pb/Pb ratios and related ages are given at the 2 σ level.

Table 2 Average chemical compositions of the studied CGM samples

	CT1	CT3	Buranga	Rongi	Coltan139	Coltan17	SN3	ZKW	DDB	HND	RL2
Major elements (% m/m)											
<i>n</i> ^a	20 ^b	22 ^b	20 ^b	20 ^b	20 ^c	10	10	10	15	10	15
WO ₃	n.d. ^d	n.d. ^d	n.d. ^d	n.d. ^d	0.74 ^d	0.53	2.07	0.24	0.45	0.56	0.22
Nb ₂ O ₅	7.08	6.25	64.40	65.68	62.58	56.92	65.45	50.80	58.51	60.88	34.81
Ta ₂ O ₅	74.72	75.46	11.59	10.96	12.67	22.31	10.38	29.95	20.74	18.53	47.18
TiO ₂	0.80	0.66	0.72	0.22	3.32	1.04	2.13	0.19	0.38	0.84	0.60
SnO ₂	0.03	0.03	0.20	0.03	0.61	0.44	0.11	0.12	0.19	0.09	0.03
Sc ₂ O ₃	n.d. ^d	n.d. ^d	n.d. ^d	n.d. ^d	0.88	b.d. ^e	0.05	b.d. ^e	b.d. ^e	b.d. ^e	b.d. ^e
FeO	14.57	14.35	10.63	14.14	10.38	10.88	17.35	5.88	7.86	11.30	10.40
MnO	0.84	0.94	9.83	6.45	8.99	8.13	2.53	12.67	11.40	8.27	6.91
Mn/(Fe + Mn)	0.06	0.06	0.48	0.32	0.47	0.43	0.13	0.69	0.60	0.43	0.40
Ta/(Nb + Ta)	0.86	0.88	0.10	0.09	0.11	0.19	0.09	0.27	0.18	0.15	0.45
Total	98.04	97.68	97.37	97.48	100.16	100.24	100.06	99.84	99.53	100.46	100.15
Trace elements ($\mu\text{g g}^{-1}$)											
<i>n</i> ^a	21	21	21	21	51	21	29	24	19	21	21
Sc	0.80	1.24	39.9	3.15	6990	7.21	407	1.95	1.59	1.34	11.6
Zn	282	344	2150	1800	356	1340	380	975	737	753	785
Y	0.18	0.27	1.84	0.66	2130	43.9	71.0	11.3	18.4	10.3	12.5
Zr	694	493	413	399	2490	1580	1850	1155	2200	2090	772
La	0.11	0.15	0.17	0.07	0.25	1.57	0.08	0.15	0.18	0.10	0.13
Ce	0.13	0.18	0.18	0.08	4.34	1.27	0.09	0.17	0.23	0.72	0.18
Pr	0.08	0.10	0.13	0.05	2.16	0.11	0.06	0.10	0.13	0.07	0.09
Nd	0.31	0.41	0.47	0.19	26.4	0.38	0.27	0.46	0.51	0.28	0.41
Sm	0.37	0.58	0.61	0.25	114	0.36	0.61	0.55	0.60	0.37	0.52
Eu	0.09	0.11	0.13	0.07	0.17	0.09	0.07	0.13	0.18	0.08	0.10
Gd	1.08	1.44	1.56	0.69	283	1.04	3.00	1.35	1.74	0.90	1.46
Tb	0.14	0.18	0.18	0.09	76.9	0.55	1.77	0.18	0.38	0.27	0.46
Dy	0.27	0.36	0.51	0.20	413	7.07	15.4	0.59	3.04	1.92	2.68
Ho	0.06	0.09	0.10	0.04	41.0	1.70	2.12	0.10	0.49	0.21	0.26
Er	0.20	0.26	0.33	0.12	75.3	6.32	5.26	0.37	1.60	0.43	0.66
Tm	0.05	0.07	0.10	0.04	10.8	1.35	0.83	0.13	0.38	0.08	0.14
Yb	0.23	0.27	0.99	0.30	78.8	12.4	5.89	1.71	3.65	0.54	1.25
Lu	0.11	0.14	0.19	0.07	9.25	1.44	0.63	0.26	0.49	0.08	0.23
Hf	328	486	97.0	29.2	363	154	145	132	231	203	127
Pb ^f	139	214.9	59.3	14.8	171	141	51.4	35.9	62.6	31.4	11.5
Th	0.03	0.04	1.54	0.12	68.1	10.3	0.83	5.72	19.1	21.2	9.47
U	268	386	285	82.7	1697	1030	711	957	1770	1060	391
REE + Sc + Y	4.19	5.83	47.3	6.06	10 200	86.7	513.5	19.5	33.6	17.7	32.6
Th/U	0.0001	0.0001	0.004	0.001	0.040	0.009	0.001	0.006	0.009	0.021	0.024

^a "*n*": number of analyses. ^b Average major element composition of samples CT1, CT3, Buranga and Rongi according to Legros *et al.*²⁵ ^c Average major element composition of sample Coltan139 according to Che *et al.*²⁹ ^d "n.d.": not determined. ^e "b.d.": below detection limit. ^f Pb ($\mu\text{g g}^{-1}$) = ²⁰⁴Pb ($\mu\text{g g}^{-1}$) + ²⁰⁶Pb ($\mu\text{g g}^{-1}$) + ²⁰⁷Pb ($\mu\text{g g}^{-1}$) + ²⁰⁸Pb ($\mu\text{g g}^{-1}$).

3 Results

3.1 Major and trace element compositions

The average chemical compositions (major and trace elements) of the studied columbite–tantanite samples are presented in Table 2. The full data set is presented in the ESI† and plotted in Fig. 1.

All EPMA analyses are plotted in Fig. 1a. The data for CT1 and CT3 plot in the ferrotapiolite field (Fig. 1a) and have relatively homogeneous compositions with average Ta/(Nb + Ta) and Mn/(Fe + Mn) atomic ratios of 0.87 and 0.06, respectively. Both samples contain minor amounts of TiO₂ (0.76–0.84% m/m and 0.56–0.72% m/m, respectively). There are seven samples (Buranga, Rongi, Coltan139, Coltan17, SN3, HND and RL2) that fall into the field of ferrocolumbite. Three of these samples show limited variation in Ta/(Nb + Ta) and Mn/(Fe + Mn) atomic ratios, whereas sample RL2 (Fig. 1a) has heterogeneous Ta/(Nb + Ta) and Mn/(Fe + Mn) atomic ratios of 0.37–0.48 and 0.35–

0.53, respectively. Samples Coltan139, Coltan17 and SN3 have high TiO₂ contents, reaching 3.32%, 1.04% and 2.13%, respectively (Table 2). Samples ZKW and DDB plot in the manganocolumbite field (Fig. 1a) and have heterogeneous Ta/(Nb + Ta) and Mn/(Fe + Mn) atomic ratios in the ranges 0.16–0.58 and 0.07–0.52, respectively.

The Th/U ratios of all samples obtained by LA-ICP-MS fall into the range of ~0.00001 to 0.01 (Fig. 1b), which overlaps with the range typically obtained for columbite–tantanite group minerals (0.001–0.1).²⁹ The Th contents are positively correlated with U contents, except for samples Buranga, CT1 and CT3 that show a large variation in Th contents, which are commonly below 0.1 μg g⁻¹.

The total REE, Sc and Y contents are below 100 μg g⁻¹ for most samples. Some samples show relatively small ranges of total REE contents, such as 2.8–3.8 μg g⁻¹ for CT1, 3.3–6.2 μg g⁻¹ for CT3, 1000–1870 μg g⁻¹ for Coltan139, and 31.3–49.0 μg g⁻¹ for SN3. The total REE, Sc and Y correlate with the U contents of

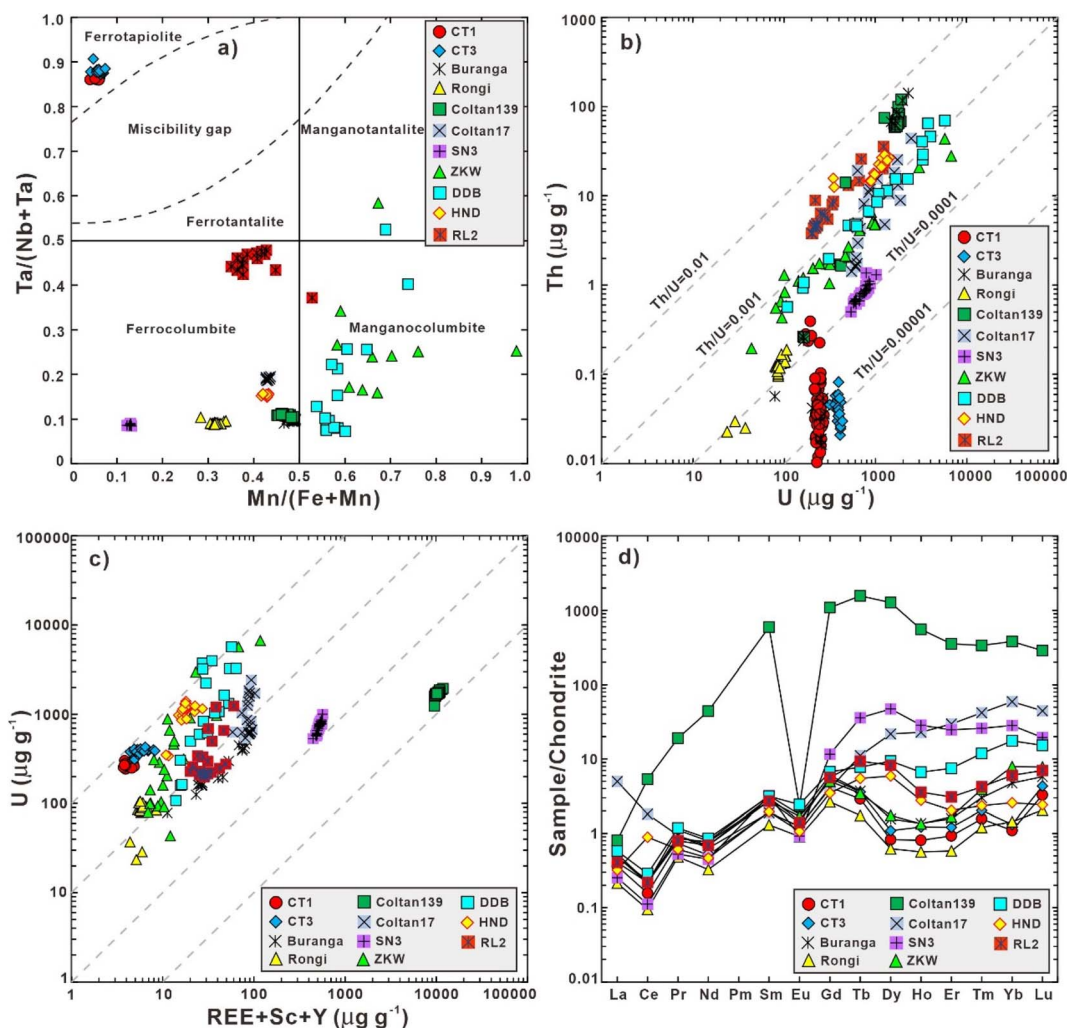


Fig. 1 Compositional characterization of the studied CGM samples. (a) Columbite–tantanite quadrilateral diagram. (b) The Th and U contents of most CGM samples are highly correlated, although with a wide range of Th/U. Samples CT1, CT3 and Buranga are unusual as they have a relatively broad range of Th contents but a narrow range of U contents. (c) For samples with a broad range of U contents, the contents of U correlate with the combined REE, Sc and Y contents. (d) Chondrite-normalized REE patterns of the CGM samples.

Table 3 ID-TIMS U–Pb analytical results for columbite

Sample ^e	Concentrations				Atomic ratios ^f				Apparent ages ^d (Ma)									
	Weight (mg)		²⁰⁶ Pb/ ²⁰⁴ Pb		Common lead (μg g ⁻¹)		²⁰⁶ Pb/ ²³⁸ U		²⁰⁷ Pb/ ²³⁵ U		²⁰⁶ Pb/ ²³⁸ U		²⁰⁷ Pb/ ²³⁵ U					
	U	Pb	measured ratios ^b	206Pb/ ²⁰⁴ Pb	U	Pb	2σ	2σ	2σ	2σ	2σ	2σ	2σ	2σ				
ZKW																		
Initial common Pb ^f : ²⁰⁶ Pb/ ²⁰⁴ Pb = 18.3 ± 0.5, ²⁰⁷ Pb/ ²⁰⁴ Pb = 15.6 ± 0.15, ²⁰⁸ Pb/ ²⁰⁴ Pb = 38.0 ± 0.5																		
C1-1	0.13	323	9.5	2820	0.2	0.319	0.0002	0.2181	0.0034	0.46	0.0496	0.0005	202.2	1.5	200.4	2.9	178.5	25.0
C1-2	0.358	71	2.2	1120	0.1	0.0321	0.0002	0.2219	0.0018	0.63	0.0501	0.0002	204.0	1.1	203.5	1.4	198.1	11.0
C1-3	0.157	172	5.3	1010	0.3	0.0321	0.0002	0.2208	0.0017	0.56	0.0499	0.0002	203.5	1.0	202.6	1.4	191.4	11.2
C1-4	0.341	254	7.7	1450	0.4	0.0318	0.0003	0.2180	0.0030	0.70	0.0497	0.0004	201.7	2.0	200.2	2.5	182.9	17.4
C1-5	0.221	207	6.2	1400	0.3	0.0315	0.0003	0.2180	0.0023	0.54	0.0506	0.0003	199.9	2.2	200.2	2.0	220.7	15.9
DDB																		
Initial common Pb ^f : ²⁰⁶ Pb/ ²⁰⁴ Pb = 18.3 ± 0.5, ²⁰⁷ Pb/ ²⁰⁴ Pb = 15.6 ± 0.15, ²⁰⁸ Pb/ ²⁰⁴ Pb = 38.0 ± 0.5																		
C2-1	0.615	478	14.0	2940	0.3	0.0315	0.0003	0.2175	0.0021	0.96	0.0500	0.0001	200.2	1.8	199.8	1.8	195.5	6.7
C2-2	0.146	480	15.1	837	1.2	0.0320	0.0003	0.2203	0.0031	0.68	0.0499	0.0005	203.1	1.9	202.1	2.6	190.9	24.5
C2-3	0.127	435	14.5	463	2.0	0.0319	0.0002	0.2163	0.0030	0.52	0.0492	0.0006	202.3	1.4	198.9	2.5	158.1	27.9
C2-4	0.120	505	15.2	2060	0.5	0.0321	0.0003	0.2184	0.0036	0.51	0.0494	0.0007	203.6	1.7	200.6	3.0	165.5	33.3
C2-5	0.112	508	15.4	1530	0.7	0.0321	0.0001	0.2206	0.0017	0.57	0.0499	0.0003	203.4	0.9	200.4	1.4	190.6	14.8
C2-6	0.152	534	15.8	2360	0.5	0.0317	0.0001	0.2182	0.0014	0.74	0.0500	0.0002	201.1	0.9	200.4	1.1	192.8	9.9
C2-7	0.243	517	15.2	2730	0.4	0.0316	0.0001	0.2182	0.0008	0.91	0.0501	0.0001	200.6	0.7	200.4	0.7	198.1	3.6
C2-8	0.149	670	19.8	3910	0.3	0.0320	0.0001	0.2197	0.0010	0.82	0.0499	0.0001	202.8	0.7	201.7	0.8	188.4	5.9
Coltani139																		
Initial common Pb ^f : ²⁰⁶ Pb/ ²⁰⁴ Pb = 18.3 ± 0.5, ²⁰⁷ Pb/ ²⁰⁴ Pb = 15.6 ± 0.15, ²⁰⁸ Pb/ ²⁰⁴ Pb = 38.0 ± 0.5																		
C3-1	0.052	1380	105.3	5720	1.3	0.0819	0.0006	0.6473	0.0053	0.87	0.0573	0.0002	507.3	3.5	506.8	3.3	504.4	8.9
C3-2	0.102	1370	104.1	12500	0.6	0.0820	0.0004	0.6479	0.0036	0.98	0.0573	0.0001	508.0	2.7	507.2	2.2	503.5	2.6
C3-3	0.092	1430	108.1	5840	1.2	0.0813	0.0007	0.6399	0.0060	0.97	0.0571	0.0001	504.1	4.4	502.2	3.7	493.7	4.8
C3-4	0.243	1400	105.7	13800	0.5	0.0820	0.0008	0.6474	0.0060	0.99	0.0573	0.0001	507.8	4.5	506.9	3.7	502.4	2.1
C3-5	0.178	1100	84.0	10100	0.6	0.0824	0.0007	0.6510	0.0053	0.99	0.0573	0.0001	510.2	4.0	509.1	3.3	503.8	2.6
C3-6	0.248	1420	107.8	10300	0.7	0.0821	0.0004	0.6489	0.0032	0.99	0.0573	0.0000	508.5	2.4	507.8	2.0	504.7	1.7

^a Small fragments, showing only fresh fracture surfaces, from single columbite crystal fragments were selected for analysis. ^b Lead isotope ratios corrected for fractionation, blank and mixed ²⁰⁵Pb–²³⁵U isotopic tracer. Samples were analyzed at GFZ German Research Centre for Geosciences, Potsdam, Germany. Total blanks were less than 15 pg for lead and less than 1 pg for uranium. ^c Lead corrected for fractionation, blank, isotopic tracer, and initial lead. ^d Apparent ages were calculated using the constants of Jaffey *et al.*⁵⁶ recommended by IUGS. ^e $\lambda^{235} = 1.55125 \times 10^{-10} \text{ y}^{-1}$, $\lambda^{238} = 9.848 \times 10^{-10} \text{ y}^{-1}$. ^f Initial lead was corrected using the Pb evolution model of Stacey and Kramers.⁴⁸

the investigated samples (Fig. 1c). Xiang *et al.*³⁴ indicate that the correlation reflects the coupled substitution of $(\text{REE}, \text{Sc}, \text{Y})^{3+} + \text{U}^{4+} \rightarrow (\text{Nb}, \text{Ta})^{5+} + (\text{Fe}, \text{Mn})^{2+}$.

The chondrite-normalised REE pattern consistently shows LREE depletions, negative Eu anomalies, and relatively flat HREE patterns (Fig. 1d). Most samples show negative Ce anomalies, except for sample HND that shows a positive Ce anomaly. Sample Coltan139 shows the most pronounced negative Eu anomaly but does not have a Ce anomaly. Sample Coltan17 is anomalous as it shows a slight La and Ce enrichment.

3.2 U–Pb ID-TIMS dating

Three CGM samples were selected for ID-TIMS U–Pb measurement as they had not been dated by applying the ID-TIMS method before (ZKW & DPB) or the complete dataset had not been reported (Coltan139). Other CGM samples have published ID-TIMS U–Pb ages.^{25,34}

3.2.1 Coltan139 (Madagascar). Six aliquots of Coltan139 ferrocolumbite were analysed using ID-TIMS. The measured $^{206}\text{Pb}/^{204}\text{Pb}$ ratios of sample Coltan139 fall in the range of 5720–13 800. Total Pb and U contents range from $84.0 \mu\text{g g}^{-1}$ to $108.1 \mu\text{g g}^{-1}$ and $1100 \mu\text{g g}^{-1}$ to $1430 \mu\text{g g}^{-1}$, respectively (Table 3). The U–Pb results overlap within analytical uncertainty and give a corrected weighted average $^{206}\text{Pb}/^{238}\text{U}$ age of $507.9 \pm 1.3 \text{ Ma}$ (2s, MSWD = 0.9; Fig. 2a). The corrected weighted average $^{207}\text{Pb}/^{206}\text{Pb}$ age of $503.3 \pm 2.7 \text{ Ma}$ (2s, MSWD = 3.9) has a relatively large uncertainty. We prefer the weighted average $^{206}\text{Pb}/^{238}\text{U}$ age that agrees with previously reported ID-TIMS ages ($\sim 506 \text{ Ma}$).¹¹

3.2.2 ZKW (Sichuan Province, China). The fragments of ZKW manganocolumbite have heterogeneous Pb and U contents that range from $2.2 \mu\text{g g}^{-1}$ to $9.5 \mu\text{g g}^{-1}$ and $71 \mu\text{g g}^{-1}$ to $323 \mu\text{g g}^{-1}$, respectively. The measured $^{206}\text{Pb}/^{204}\text{Pb}$ ratios range from 1010 to 2820 (Table 3). The apparent $^{206}\text{Pb}/^{238}\text{U}$ ages of the five fragments range from 199.9 ± 2.2 to $204.0 \pm 1.1 \text{ Ma}$ and yield a weighted average $^{206}\text{Pb}/^{238}\text{U}$ age of $203.0 \pm 1.6 \text{ Ma}$ (2s, MSWD = 3.7; Fig. 2b). The relatively large uncertainty might have been caused by inclusions with common Pb (such as sulphides or feldspar) and the presence of metamict domains that had not been removed completely during the leaching process. Fei *et al.*³⁷ documented the intergrowth of CGM with feldspar in columbite from ZKW and DDB.

3.2.3 DDB (Sichuan Province, China). Sample DDB, which was sampled from the same ore field as sample ZKW, shows $^{206}\text{Pb}/^{204}\text{Pb}$ values ranging from 463 to 3910 (Table 3). The fragments of DDB manganocolumbite have higher Pb and U contents, ranging from $14.0 \mu\text{g g}^{-1}$ to $19.8 \mu\text{g g}^{-1}$ and $435 \mu\text{g g}^{-1}$ to $670 \mu\text{g g}^{-1}$, respectively. The apparent $^{206}\text{Pb}/^{238}\text{U}$ ages of the eight fragments range from 200.0 ± 1.8 to $203.6 \pm 1.7 \text{ Ma}$ and yield a weighted average $^{206}\text{Pb}/^{238}\text{U}$ age of $202.0 \pm 1.0 \text{ Ma}$ (2s, MSWD = 1.3; Fig. 2c). The large variation of the measured $^{206}\text{Pb}/^{204}\text{Pb}$ values of sample DDB reflects the presence of inclusions carrying common Pb that have not been completely removed during the sample preparation using dilute HF.

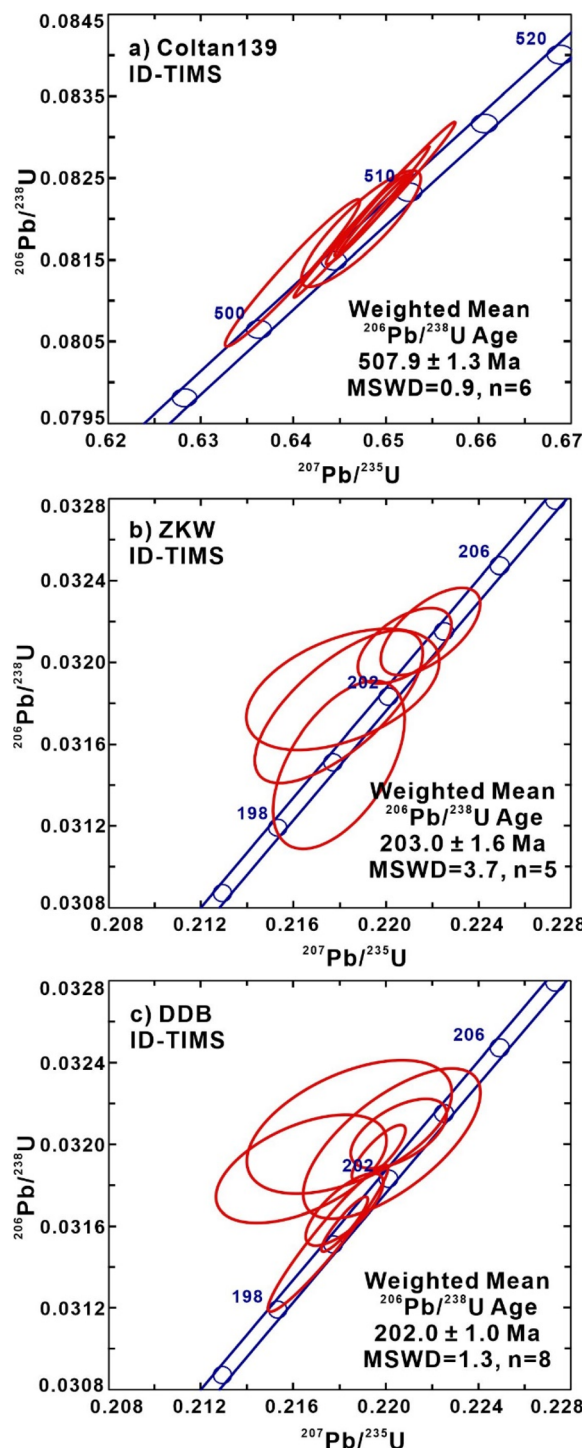


Fig. 2 U–Pb concordia diagram for CGM ID-TIMS data. All error ellipses are given at the 2-sigma level.

3.3 LA-ICP-MS U–Pb dating

In this study, the *in situ* U–Pb ages of the CGM samples are shown in Fig. 3–5 and reported in two different ways. Concordia diagrams are presented for radiogenic samples with little common Pb (such as CT3 and Buranga). For other samples with variable common Pb contents, all data are plotted in Tera–Wasserburg diagrams and presented as discordia forced

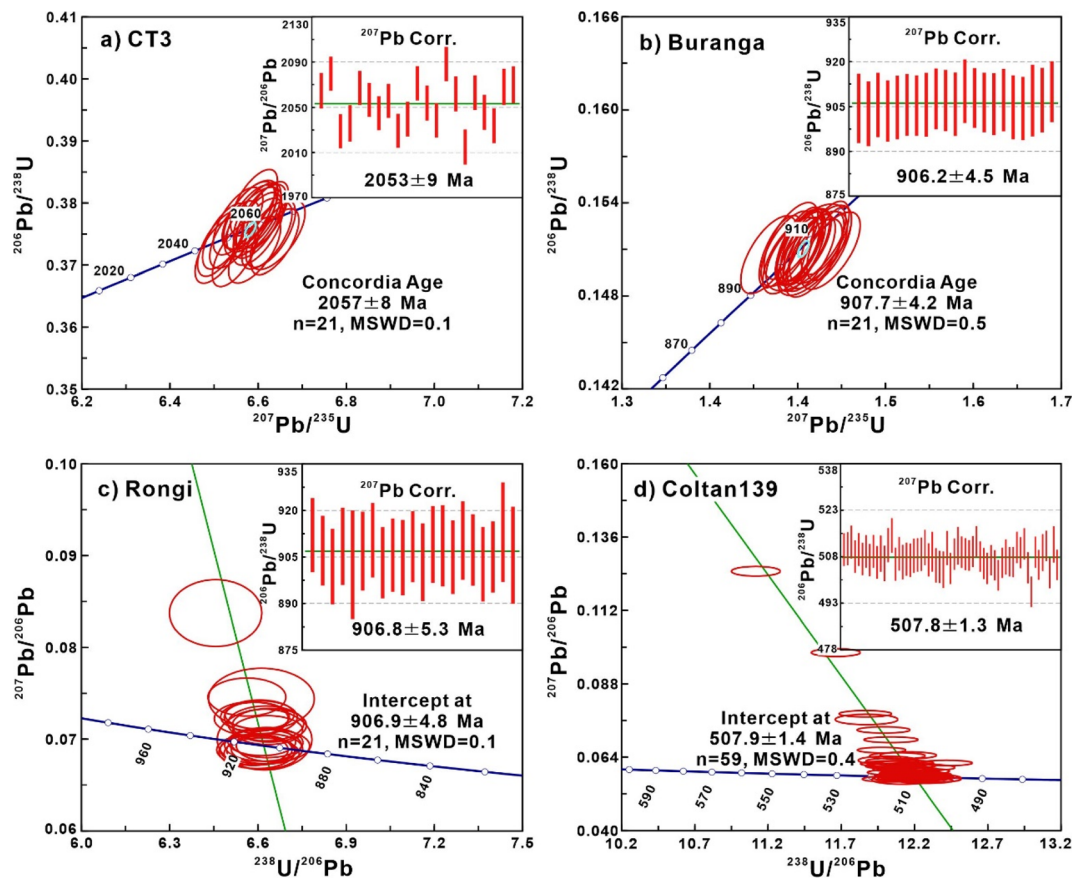


Fig. 3 Concordia diagrams for (a) CT3 (ID-TIMS:²⁵ 2053.2 ± 1.3 Ma) and (b) Buranga (ID-TIMS:²⁵ 905.2 ± 3.2 Ma). Tera–Wasserberg diagrams for (c) Rongi (SIMS:²⁵ 905.0 ± 5.0 Ma) and (d) Coltan139 (ID-TIMS from this study: 507.9 ± 1.3 Ma). Insets show the weighted mean and ²⁰⁷Pb/²⁰⁶Pb age for (a) CT3 and ²⁰⁶Pb/²³⁸U ages for (b) Buranga, (c) Rongi and (d) Coltan139. The discordia in the Tera–Wasserberg diagrams is forced through ²⁰⁷Pb/²⁰⁶Pb ratios estimated using the Stacey and Kramers⁴⁸ crustal Pb model. “*n*” represents the number of analyses. Error ellipses are shown at the 95% confidence level.

through a ²⁰⁷Pb/²⁰⁶Pb ratio estimated from Stacey and Kramers⁴⁸ crustal Pb model. For the calculation of the discordia, we used an uncertainty of 2% for the ²⁰⁷Pb/²⁰⁶Pb ratio of the model Pb.

3.3.1 CT3 (Ivory Coast). In the Wetherill diagram, most data of sample CT3 cluster near the concordia curve and yield a concordia age of 2057 ± 8 Ma (2*s*, MSWD = 0.1, *n* = 21; Fig. 3a). Weighted mean ²⁰⁷Pb/²⁰⁶Pb age is 2053 ± 9 Ma (2*s*, MSWD = 1.5, *n* = 21; Fig. 3a), and weighted mean ²⁰⁶Pb/²³⁸U age is 2054 ± 10 Ma (2*s*, MSWD = 0.2, *n* = 21). This result agrees well with the published ID-TIMS age of 2053.2 ± 1.3 Ma (2*s*, MSWD = 2.2)²⁵ and SIMS age of 2054.1 ± 2.2 Ma (2*s*, MSWD = 1.4).²⁵

3.3.2 Buranga and Rongi (Rwanda). Sample Buranga is a radiogenic ferrocolumbite. Twenty-one analyses of sample Buranga yielded a concordia age of 907.7 ± 4.2 Ma (2*s*, MSWD = 0.5, *n* = 21; Fig. 3b) and a weighted mean ²⁰⁶Pb/²³⁸U age of 906.2 ± 4.5 Ma (2*s*, MSWD = 0.1, *n* = 21; Fig. 3b). This result agrees well with the reported ID-TIMS age of 905.2 ± 3.2 Ma (2*s*, MSWD = 0.4).²⁵

Sample Rongi shows small variations in the contribution of common Pb and has *f*₂₀₆ values ranging from 0 to 1.74%. The

discordia yields an intercept age of 906.9 ± 4.8 Ma (2*s*, MSWD = 0.1, *n* = 21; Fig. 3c). The chosen ²⁰⁷Pb/²⁰⁶Pb model ratio of 0.90 (ref. 48) is slightly higher than the unconstrained intercept of 0.80 ± 0.16, which corresponds to an intercept age of 907.0 ± 11.0 Ma (2*s*, MSWD = 0.1, *n* = 21). Both ages agree with each other within uncertainties. The ²⁰⁷Pb corrected weighted average ²⁰⁶Pb/²³⁸U age is 906.8 ± 5.8 Ma (2*s*, MSWD = 0.1, *n* = 21; Fig. 3c). The laser ablation result of Rongi agrees well with the published age of 905.0 ± 5.0 Ma (2*s*, MSWD = 0.9).²⁵

3.3.3 Coltan139 (Madagascar). A total of fifty-nine analyses of sample Coltan139 define an anchored discordia on the Tera–Wasserberg diagram with an intercept age of 507.9 ± 1.4 Ma (2*s*, MSWD = 0.4, *n* = 59; Fig. 3d). For comparison, the unconstrained discordia in the dataset yields a ²⁰⁷Pb/²⁰⁶Pb intercept of 0.85 ± 0.05 and an age of 507.8 ± 2.7 Ma (2*s*, MSWD = 0.1, *n* = 59; Fig. 3d). This sample shows a wide range of common Pb contributions with *f*₂₀₆ reaching up to 8.29%. The weighted mean ²⁰⁶Pb/²³⁸U age of 507.8 ± 1.3 Ma (2*s*, MSWD = 0.4, *n* = 21; Fig. 3d) agrees well with published values (~506 Ma)¹¹ and the ID-TIMS results reported in this study.

3.3.4 Coltan17 (Brazil). Among the investigated samples, Coltan17 has the highest contribution of common Pb and has

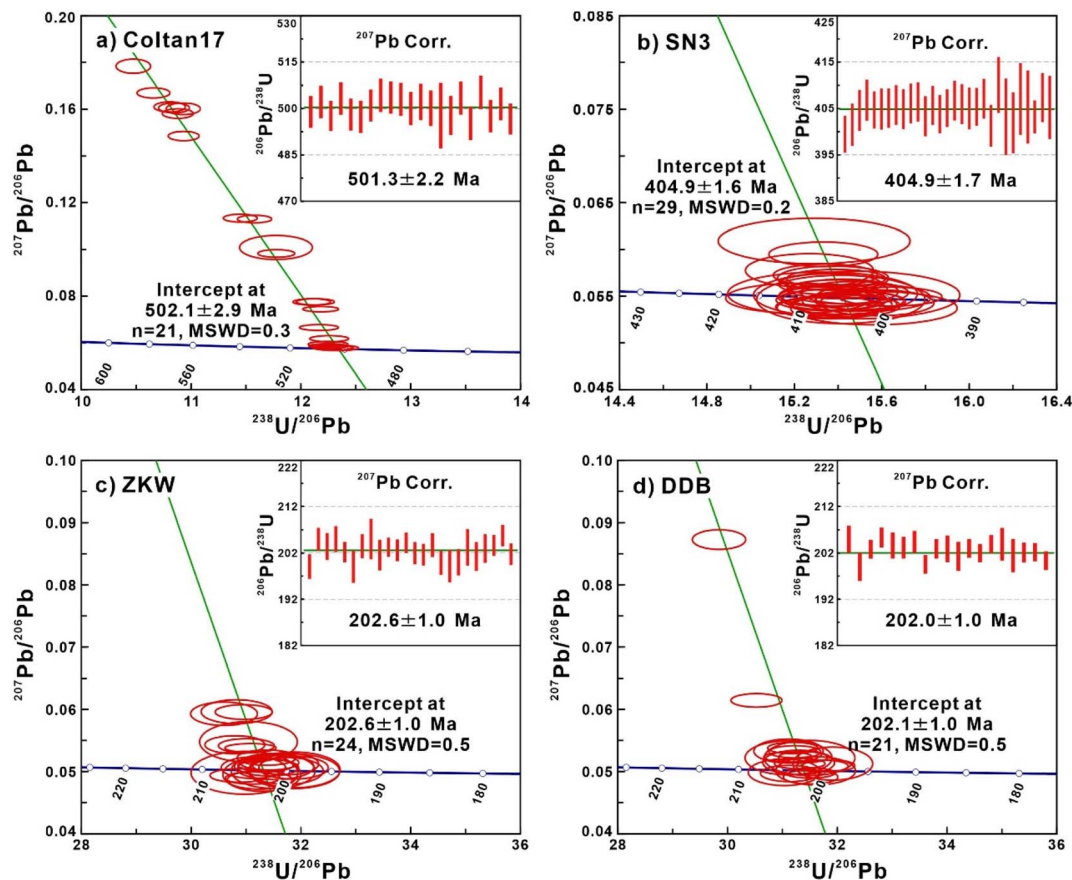


Fig. 4 Tera–Wasserburg diagrams for (a) Coltan17, (b) SN3 (ID-TIMS:³⁴ 404.0 ± 1.3 Ma), (c) ZKW (ID-TIMS from this study: 203.0 ± 1.6 Ma) and (d) DDB (ID-TIMS from this study: 202.0 ± 1.0 Ma). Insets show ²⁰⁷Pb corrected weighted mean ²⁰⁶Pb/²³⁸U ages for (a) Coltan17, (b) SN3, (c) ZKW and (d) DDB. The discordias on the Tera–Wasserburg diagrams are forced through ²⁰⁷Pb/²⁰⁶Pb ratios estimated using the crustal Pb model of Stacey and Kramers.⁴⁸ “n” represents the number of analyses. Error ellipses are shown at the 95% confidence level.

f_{206} values ranging from 0.05% to 14.90%. The discordia constrained by 21 analyses yields on the Tera–Wasserburg diagram an age of 502.1 ± 2.9 Ma (2s, MSWD = 0.3, n = 21; Fig. 4a). The corresponding ²⁰⁷Pb corrected weighted mean ²⁰⁶Pb/²³⁸U age is 501.3 ± 2.2 Ma (2s, MSWD = 0.3, n = 21; Fig. 4a). The unanchored data give an upper intercept ²⁰⁷Pb/²⁰⁶Pb ratio of 0.89 ± 0.06 and an intercept age of 502.7 ± 3.1 Ma (2s, MSWD = 0.3, n = 21). The obtained ages agree well with the published age of ~502 Ma.^{10,32}

3.3.5 SN3 (Shanxi Province, China). Most analyses of sample SN3 fall on the concordia on the Tera–Wasserburg diagram, *i.e.*, have hardly any contributions of common Pb, which is expressed in f_{206} values less than 0.76%. The discordia constrained by twenty-nine analyses yields an intercept age of 404.9 ± 1.6 Ma (2s, MSWD = 0.2, n = 29; Fig. 4b) on a Tera–Wasserburg diagram. The corresponding ²⁰⁷Pb corrected weighted mean ²⁰⁶Pb/²³⁸U age is 404.9 ± 1.7 Ma (2s, MSWD = 0.1, n = 29; Fig. 4b). The laser ablation U–Pb age agrees well with the ID-TIMS determined result of 404.0 ± 1.3 Ma (2s, MSWD = 2.2).³⁴

3.3.6 ZKW and DDB (Sichuan Province, China). Sample ZKW shows limited variation in common Pb contributions with f_{206} varying from 0 to 1.19%. The laser ablation U–Pb results

define an intercept age of 202.6 ± 1.0 Ma (2s, MSWD = 0.5, n = 24; Fig. 4c). The ²⁰⁷Pb corrected weighted mean ²⁰⁶Pb/²³⁸U age is 202.6 ± 1.0 Ma (2s, MSWD = 0.5, n = 24; Fig. 4c). For comparison, the unconstrained discordia yields an ²⁰⁷Pb/²⁰⁶Pb intercept of 0.57 ± 0.84 and an age of 202.3 ± 2.5 Ma (2s, MSWD = 0.1, n = 24). As the twenty-four U–Pb analyses of sample ZKW plot on or very close to the concordia, the ²⁰⁷Pb/²⁰⁶Pb intercept is not well constrained.

Analyses of sample DDB show more variable common Pb contributions than sample ZKW from the same deposit. The f_{206} values of DDB range from 0 to 4.65%. The dataset of ZKW yields an intercept age of 202.1 ± 1.0 Ma (2s, MSWD = 0.5, n = 21; Fig. 4d) and a ²⁰⁷Pb corrected weighted mean ²⁰⁶Pb/²³⁸U age of 202.0 ± 1.0 Ma (2s, MSWD = 0.5, n = 21; Fig. 4d). The unconstrained discordia intercepts at a ²⁰⁷Pb/²⁰⁶Pb ratio of 0.75 ± 0.52 and yields an age of 201.9 ± 2.2 Ma (2s, MSWD = 0.1, n = 21). The large uncertainty of the ²⁰⁷Pb/²⁰⁶Pb ratio reflects the small spread of the data that falls close to the concordia.

The U–Pb ages of ZKW and DDB determined by LA-ICP-MS agree well with the published mineralization age of ~200 Ma.^{37,38}

3.3.7 HND and RL2 (The junction of Hunan and Hubei Province, China). Twenty-one analyses of sample HND yield an

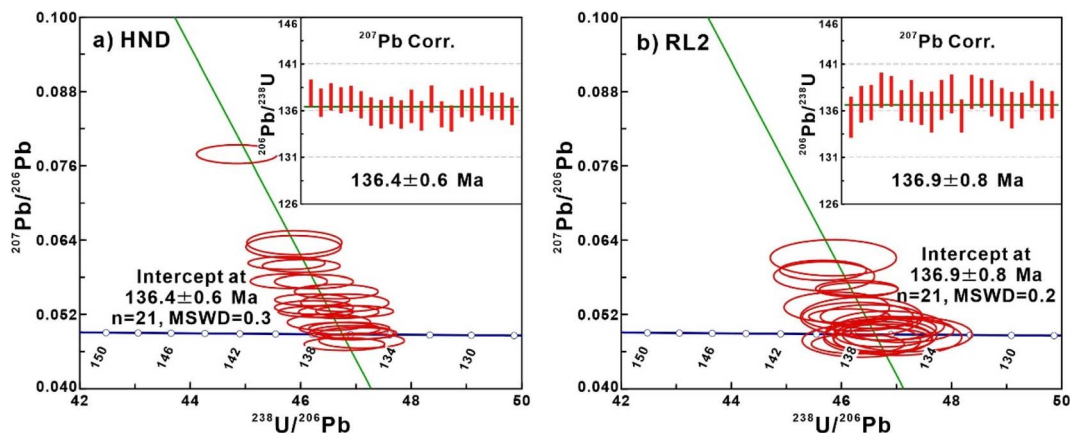


Fig. 5 Tera–Wasserburg diagrams for (a) HND (ID-TIMS:³⁴ 136.2 ± 0.9 Ma) and (b) RL2 (ID-TIMS:³⁴ 135.7 ± 0.3 Ma). Insets show ²⁰⁷Pb corrected weighted mean ²⁰⁶Pb/²³⁸U age for (a) HND and (b) RL2. Discordia in Tera–Wasserburg diagrams is forced through ²⁰⁷Pb/²⁰⁶Pb ratios estimated using the crustal Pb model of Stacey and Kramers.⁴⁸ “n” represents the number of analyses. Error ellipses are given at the 95% confidence level.

intercept age of 136.4 ± 0.6 Ma (2s, MSWD = 0.3, n = 21; Fig. 5a). The corresponding ²⁰⁷Pb corrected weighted mean ²⁰⁶Pb/²³⁸U age is 136.4 ± 0.6 Ma (2s, MSWD = 0.3, n = 21; Fig. 5a). The unconstrained discordia yields a ²⁰⁷Pb/²⁰⁶Pb intercept of 0.69 ± 0.53 and an intercept age of 136.2 ± 1.6 Ma (2s, MSWD = 0.1, n = 21). The relatively large uncertainty of the unconstrained ²⁰⁷Pb/²⁰⁶Pb intercept reflects the limited spread of the dataset, which is also reflected in the small range of *f*₂₀₆ from 0 to 1.86%.

Sample RL2 also contains very little common Pb with *f*₂₀₆ varying from 0 to 1.55%. The laser ablation U–Pb data are defined on the Tera–Wasserburg diagram as an intercept age of 136.9 ± 0.9 Ma (2s, MSWD = 0.2, n = 21; Fig. 5b). The corresponding ²⁰⁷Pb corrected weighted mean ²⁰⁶Pb/²³⁸U age is 136.9 ± 0.8 Ma (2s, MSWD = 0.2, n = 21; Fig. 5b). The unconstrained regression line through the dataset yields a ²⁰⁷Pb/²⁰⁶Pb intercept of 0.63 ± 0.95 and an intercept age of 136.7 ± 2.0 Ma (2s, MSWD = 0.1, n = 21).

The *in situ* U–Pb ages of HND and RL2 obtained in this study agree well with the published ID-TIMS age of ~136 Ma.³⁴

4 Discussion

4.1 Matrix effect related to Ta/(Nb + Ta) and Mn/(Fe + Mn) atomic ratios

Reference materials are crucial for microanalysis to obtain reliable results. In this study, we used ferrotapiolite CT1 as the primary reference material. CT1 has Ta/(Nb + Ta) and Mn/(Fe + Mn) atomic ratios of 0.86 and 0.06, respectively, and was used to calibrate the U/Pb ratios of other CGM crystals that have Ta/(Nb + Ta) and Mn/(Fe + Mn) atomic ratios ranging from 0.09 to 0.88 and from 0.06 to 0.69, respectively. The obtained LA-ICP-MS U–Pb ages of these normalized samples agree well with their ID-TIMS U–Pb ages presented here and reported earlier (Fig. 3–5). Thus, for the analytical conditions used in this study (Table 1), large variations in the major element composition of the CGM crystals have little or no effect on the accuracy of the obtained LA-ICP-MS U–Pb ages.

The variation in Mn/(Fe + Mn) does not affect the accuracy of LA-ICP-MS U–Pb ages because Fe and Mn have similar masses. Such insensitivity to the composition was also reported for LA-ICP-MS U–Pb dating of wolframite series minerals.²³ In contrast, the large mass difference between Nb and Ta may introduce a significant matrix effect, largely depending on the used method and analytical settings. For instance, the matrix effect due to variations in Ta/(Nb + Ta) may have induced apparent discordance in the SIMS data.²⁵ As matrix effects in CGM U–Pb dating were not consistently observed in LA-ICP-MS studies,^{26,31} favourable analytical settings may minimize matrix effects. The use of femtosecond laser ablation systems (lower heating effect and smaller aerosol particles^{49,50}), wet plasma conditions (increasing plasma robustness^{51–53}), and some ablation modes (such as line scanning mode, low laser energy density and moderate ablation spot size^{29,34}) have been reported to minimize matrix effects.

4.2 Re-evaluation of Coltan139 as a reference material

Ferrocolumbite Coltan139 has been used as a reference material for *in situ* columbite–tantalite mineral U–Pb dating for over a decade.^{9–11,20,29,32,54,55} The ID-TIMS U–Pb age of this sample was determined in two laboratories and was reported by Melcher *et al.*¹¹ although the ID-TIMS data were not published. In this study, we dated sample Coltan139 using the ID-TIMS U–Pb method and reported the results (Table 3). The reported ID-TIMS ages agree with the previously reported age of ~506 Ma.¹¹

Fig. 6 shows the deviation in the ²⁰⁷Pb/²⁰⁶Pb, ²⁰⁶Pb/²³⁸U and ²⁰⁷Pb/²³⁵U ratios of Coltan139 as determined by LA-ICP-MS from the corresponding ratios determined by ID-TIMS. The deviation is typically less than 5% from the ID-TIMS value and is due to common Pb contributions rather than Pb loss. Although all Coltan139 fragments are derived from one single crystal,¹¹ the deviation is considerably larger than that previously reported (less than 3%).^{29,34} This may reflect the fact that common Pb contents differ within the individual shards of this crystal and among different shards. Therefore, special care (such as

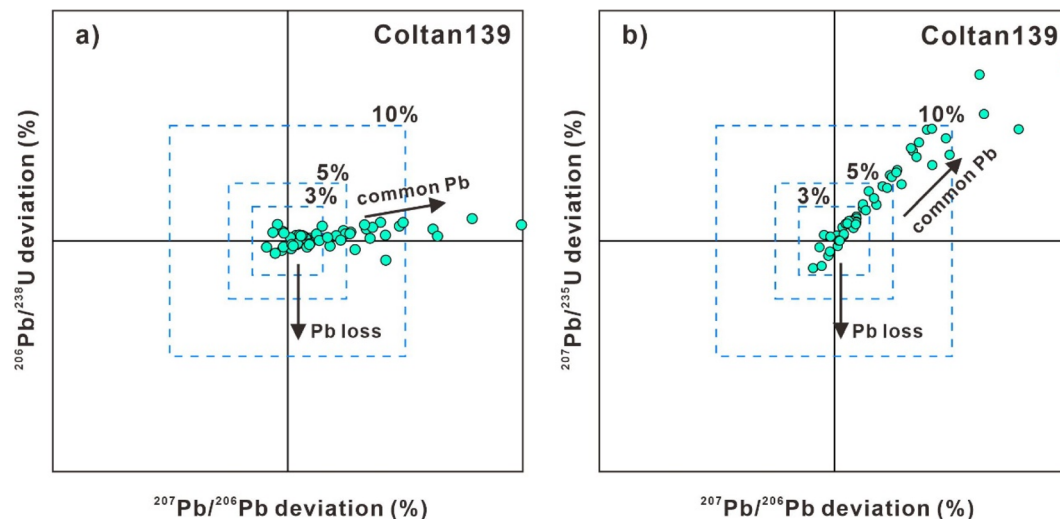


Fig. 6 Deviation of U/Pb isotope ratios of sample Coltan139 determined by LA-ICP-MS from the corresponding ratios determined by ID-TIMS. (a) Plot of $^{206}\text{Pb}/^{238}\text{U}$ deviation versus $^{207}\text{Pb}/^{206}\text{Pb}$ deviation. (b) Plot of $^{207}\text{Pb}/^{235}\text{U}$ deviation versus $^{207}\text{Pb}/^{206}\text{Pb}$ deviation.

back-scattered electron images, trace elements and real-time mass spectrum signals) should be taken when using Coltan139 as a reference material for *in situ* U–Pb dating.

4.3 Potential CGM reference materials for *in situ* U–Pb dating

The results of the LA-ICP-MS U–Pb dating of the investigated CGM samples are presented in Table 4. The tested columbite–tantanalite minerals typically have U and Pb contents varying from $83 \mu\text{g g}^{-1}$ to $1560 \mu\text{g g}^{-1}$ and from $15 \mu\text{g g}^{-1}$ to $215 \mu\text{g g}^{-1}$, respectively. Among the investigated samples, Coltan139 is the most commonly used reference material for laser ablation U–Pb dating,²⁹ even though the common Pb contents of Coltan139 samples vary throughout the crystal (Fig. 3d and 6). Therefore, special care should be taken when using Coltan139 as the primary reference material. In contrast, CGM samples CT3, Buranga and Rongi investigated by Legros *et al.*²⁵ have negligible

or small contributions of common Pb and show very good reproducibility. The LA-ICP-MS U–Pb ages of these three CGM samples agree well with the reported ID-TIMS and SIMS ages.²⁵ As depicted in Fig. 7a–c, samples CT3, Buranga and Rongi are used as primary reference materials to calibrate CT1 and Coltan139. The obtained ages are consistent with recommended results, indicating that samples CT3, Buranga and Rongi can serve as primary reference materials and may be preferable to Coltan139. Samples SN3, HND and RL2 were investigated by Xiang *et al.*³⁴ Each of these CGM samples exhibits limited variation in the common Pb contents. The LA-ICP-MS ages obtained in this study are consistent with reported ID-TIMS results.³⁴ Sample SN3 contains very little common Pb and can be used as a primary reference material (Fig. 7d; an example of SN3 used as a primary reference material). Samples HND and RL2 contain minor amounts of common Pb and obtain robust intercept ages on Tera–Wasserburg diagrams. They can also be used as reference materials.⁵⁷ Data from samples ZKW and DDB have not

Table 4 Compilation of columbite–tantanalite group minerals U–Pb ages obtained by LA-ICP-MS in this study^a

Sample	$\mu\text{g g}^{-1}$				Data for Tera–Wasserburg plot		Data for Wetherill plot		f ₂₀₆ ^d (%)		207Pb corr. (Ma)	
	n ^b	Pb ^c	Th	U	Th/U	²³⁸ U/ ²⁰⁶ Pb 2s	²⁰⁷ Pb/ ²⁰⁶ Pb 2s	²⁰⁷ Pb/ ²³⁵ U 2s	²⁰⁶ Pb/ ²³⁸ U 2s	f ₂₀₆ ^d 2s	²⁰⁶ Pb/ ²³⁸ U 2s	2s _{sys} ^e
CT3	21	215	0.04	386	0.0001	2.66	0.032 0.127	0.003 6.584	0.076 0.3758	0.0045 0.13	0.25 2054	21 46
Buranga	21	147	33.0	820	0.019	6.62	0.029 0.069	0.002 1.445	0.025 0.1510	0.0007 0.09	0.14 906	3.8 19
Rongi	21	15	0.12	83	0.001	6.60	0.080 0.071	0.007 1.489	0.160 0.1514	0.0019 0.27	0.80 907	6.4 19
Coltan139	59	158	60.5	1564	0.036	12.13	0.364 0.062	0.021 0.710	0.292 0.0825	0.0026 0.58	2.61 508	6.3 12
Coltan17	21	141	10.3	1030	0.009	11.64	1.328 0.105	0.090 1.267	1.221 0.0862	0.0101 5.89	11.0 501	5.4 11
SN3	29	51	0.83	711	0.001	15.41	0.191 0.055	0.003 0.498	0.032 0.0649	0.0008 0.11	0.38 405	4.4 9.1
ZKW	24	36	5.72	957	0.006	31.28	0.420 0.735	0.001 0.007	0.035 0.0320	0.0008 0.27	0.79 202	3.9 5.6
DDB	19	63	19.1	1774	0.009	31.27	0.940 0.054	0.017 0.239	0.092 0.0320	0.0010 0.47	2.12 202	3.4 5.2
HND	21	31	21.2	1064	0.021	46.39	1.125 0.055	0.014 0.166	0.051 0.0216	0.0005 0.81	1.75 136	1.5 3.1
RL2	21	12	9.47	391	0.024	46.45	0.886 0.052	0.008 0.154	0.028 0.0215	0.0004 0.39	0.98 137	1.8 3.2

^a Mass fraction's uncertainties are about 20%. Decay constants of Jaffey *et al.*⁵⁶ were used. ^b “n”: number of analyses. ^c Pb ($\mu\text{g g}^{-1}$) = ^{204}Pb ($\mu\text{g g}^{-1}$) + ^{206}Pb ($\mu\text{g g}^{-1}$) + ^{207}Pb ($\mu\text{g g}^{-1}$) + ^{208}Pb ($\mu\text{g g}^{-1}$). ^d f₂₀₆, common ^{206}Pb in total ^{206}Pb ; $f_{206} = [(^{207}\text{Pb}/^{206}\text{Pb})_{\text{total}} - (^{207}\text{Pb}/^{206}\text{Pb})_{\text{radiogenic}}] / [(^{207}\text{Pb}/^{206}\text{Pb})_{\text{initial}} - (^{207}\text{Pb}/^{206}\text{Pb})_{\text{radiogenic}}]$. ^e Total systematic uncertainties (s_{sys}): $^{206}\text{Pb}/^{238}\text{U} = 2.0\%$ (2s).

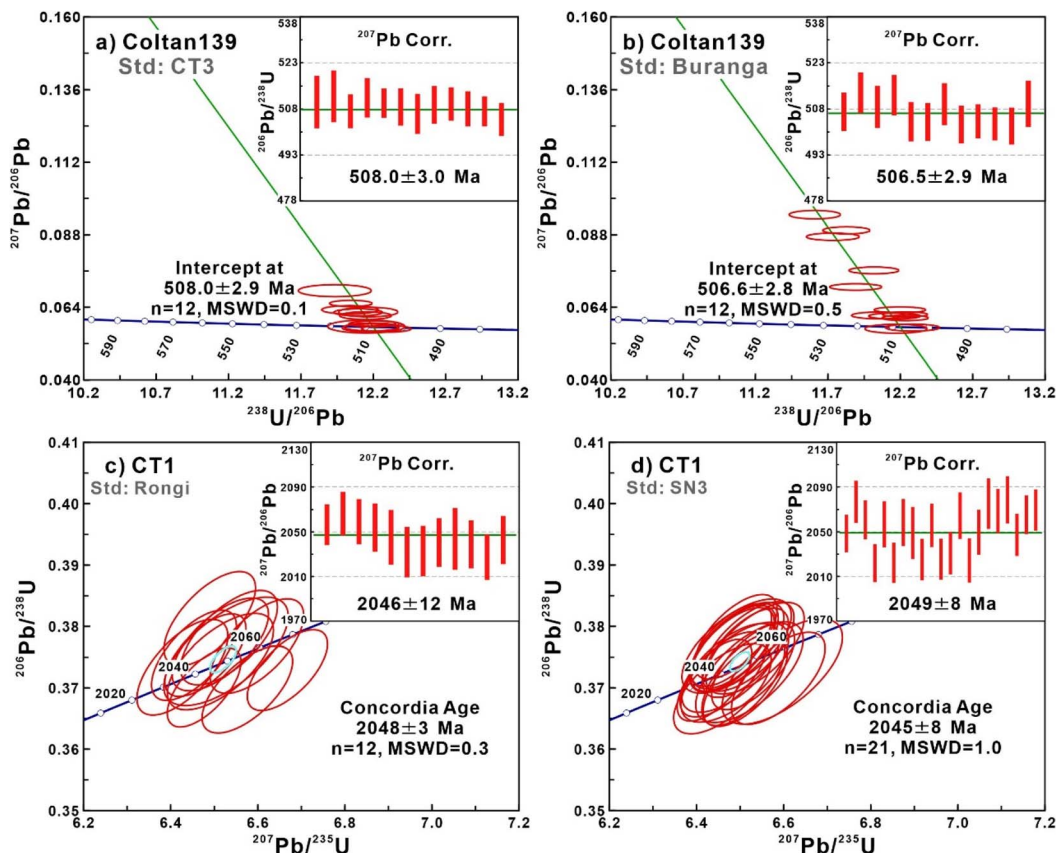


Fig. 7 U–Pb and Tera–Wasserburg (a and b) and concordia (c and d) diagrams for columbite–tantalite LA-ICP-MS data. Calibration using different reference materials yields intercept ages, concordia ages, and ^{207}Pb corrected weighted mean $^{207}\text{Pb}/^{206}\text{Pb}$ and $^{206}\text{Pb}/^{238}\text{U}$ ages. Discordias on Tera–Wasserburg diagrams are forced through $^{207}\text{Pb}/^{206}\text{Pb}$ ratios estimated using the crustal Pb model of Stacey and Kramers.⁴⁸ “n” represents the number of analyses. Error ellipses are given at the 95% confidence level.

been reported before. Both samples show small variations in the common Pb contents, resulting in f_{206} values of less than 5%. The U–Pb ages obtained by LA-ICP-MS are consistent with ID-TIMS ages and published cassiterite and columbite ages.^{37,38} They are suitable as reference materials for CGM U–Pb dating. In contrast, sample Coltan17 contains high and variable common Pb contents and yields a robust U–Pb age. Coltan17, however, needs to be dated by applying the ID-TIMS method. Therefore, it should be used presently only as secondary reference material to check the data quality.

5 Conclusions

We characterize columbite–tantalite minerals with a broad range of compositions and ages from 2054 Ma to 136 Ma. The U–Pb dating of columbite–tantalite minerals by LA-ICP-MS indicates that compositional variations in Ta/Nb and Mn/Fe do not affect the fractionation behaviour of U and Pb. Three CGM samples Coltan139, ZKW and DDB yield ID-TIMS $^{206}\text{Pb}/^{238}\text{U}$ ages of 507.9 ± 1.3 Ma (2s), 203.0 ± 1.6 Ma (2s) and 202.0 ± 1.0 Ma (2s), respectively. The homogeneity of Coltan139 was examined, which revealed relatively high common Pb contents. We recommend CGM samples CT3, Buranga, Rongi and SN3 as primary reference materials for *in situ* CGM

U–Pb dating. Samples ZKW, DDB, HND and RL2 have relatively high common Pb contents but yield robust U–Pb ages. They can also serve as primary reference materials. Coltan17 contains a considerable amount of common Pb but yields a robust intercept age. The age of this CGM sample needs to be verified using the ID-TIMS method. At present, it may serve as a secondary reference material.

Data availability

The data that support the findings of this study are available in the online ESI of this article.†

Author contributions

Conceptualization, M. Y. and Y.-H. Y.; investigation, M. Y.; formal analysis, M. Y.; methodology, Y.-H. Y.; supervision, Y.-H. Y. and R.-L. R.; writing – original draft, M. Y.; writing – review & editing, R.-L. R., F.-Y. W., R.-C. W., X. D. C., G. C. F., Y. D. and T. W.; funding acquisition, Y.-H. Y. and M. Y.

Conflicts of interest

The authors declare no conflict of interest.

Acknowledgements

This study was supported by the National Key R&D Program of China (grant no. 2018YFA0702600), State Key Laboratory of Lithospheric Evolution, Institute of Geology and Geophysics, Chinese Academy of Sciences (grant no. SKL-Z202304), Natural Science Foundation of China (grants no. 42173034) and Research Startup Funding from Hainan Institute of Zhejiang University (grant no. 0212-6602-A12201). We are indebted to Gäbler H. E. for providing Coltan139 and Coltan17, Legros H. and Mercadier J. for providing CT1, CT3, Buranga and Rongi, Xiang L. for providing SN3, HND and RL2. Small aliquots of samples ZKW and DDB may be obtained from Yue-Heng Yang.

References

- 1 R. Baumgartner, R. L. Romer, R. Moritz, R. Sallet and M. Chiaradia, *Can. Mineral.*, 2006, **44**, 69–86.
- 2 R. L. Linnen, M. Van Lichtervelde and P. Černý, *Elements*, 2012, **8**, 275–280.
- 3 Z. Y. Zhu, R. C. Wang, X. D. Che, J. C. Zhu, X. L. Wei and X. E. Huang, *Ore Geol. Rev.*, 2015, **65**, 749–760.
- 4 R. L. Romer and J. E. Wright, *Geochim. Cosmochim. Acta*, 1992, **56**, 2137–2142.
- 5 R. L. Romer and S. A. Smeds, *Precambrian Res.*, 1994, **67**, 141–158.
- 6 R. L. Romer and B. Lehmann, *Econ. Geol.*, 1995, **90**, 2303–2309.
- 7 S. R. Smith, G. L. Foster, R. L. Romer, A. G. Tindle, S. P. Kelley, S. R. Noble, M. Horstwood and F. W. Breaks, *Contrib. Mineral. Petrol.*, 2004, **147**, 549–564.
- 8 T. Geisler, R. T. Pidgeon, W. van Bronswijk and R. Kurtz, *Chem. Geol.*, 2002, **191**, 141–154.
- 9 Y. G. Feng, T. Liang, R. Linnen, Z. Zhang, Y. Zhou, Z. L. Zhang and J. G. Gao, *Lithos*, 2020, **362–363**, 105461.
- 10 H. E. Gäbler, F. Melcher, T. Graupner, A. Bahr, M. A. Sitnikova, F. Henjes-Kunst, T. Oberthür, H. Brätz and A. Gerdes, *Geostand. Geoanal. Res.*, 2011, **35**, 431–448.
- 11 F. Melcher, T. Graupner, H. E. Gäbler, M. Sitnikova, F. Henjes-Kunst, T. Oberthür, A. Gerdes and S. Dewaele, *Ore Geol. Rev.*, 2015, **64**, 667–719.
- 12 F. Melcher, T. Graupner, H. E. Gäbler, M. Sitnikova, T. Oberthür, A. Gerdes, E. Badanina and T. Chudy, *Ore Geol. Rev.*, 2017, **89**, 946–987.
- 13 L. T. Aldrich, G. L. Davis, G. R. Tilton and G. W. Wetherill, *J. Geophys. Res.*, 1956, **61**, 215–232.
- 14 R. L. Romer, *Contrib. Mineral. Petrol.*, 2003, **145**, 481–491.
- 15 R. L. Romer and S. A. Smeds, *Precambrian Res.*, 1996, **76**, 15–30.
- 16 R. L. Romer and S. A. Smeds, *Precambrian Res.*, 1997, **82**, 85–99.
- 17 R. L. Romer, S. A. Smeds and P. Cerny, *Mineral. Petrol.*, 1996, **57**, 243–260.
- 18 R. L. Romer, N. Nowaczyk and R. Wirth, *Int. J. Earth Sci.*, 2007, **96**, 375–387.
- 19 A. Lindroos, R. L. Romer, C. Ehlers and R. Alviola, *Terra Nova*, 1996, **8**, 567–574.
- 20 D. J. Kontak, R. A. Creaser, L. M. Heaman and D. A. Archibald, *Atl. Geol.*, 2005, **41**, 17–29.
- 21 D. Küster, R. L. Romer, D. Tolessa, D. Zerihun, K. Bheemalingeswara, F. Melcher and T. Oberthür, *Miner. Deposita*, 2009, **44**, 723–750.
- 22 A. Müller, R. L. Romer and R. B. Pedersen, *Can. Mineral.*, 2017, **55**, 1–33.
- 23 M. Yang, Y. H. Yang, S. T. Wu, R. L. Romer, X. D. Che, Z. F. Zhao, W. S. Li, J. H. Yang, F. Y. Wu, L. W. Xie, C. Huang, D. Zhang and Y. Zhang, *J. Anal. At. Spectrom.*, 2020, **35**, 2191–2203.
- 24 Y. H. Yang, M. Yang, H. Wang, J. H. Yang and F. Y. Wu, *Sci. China: Earth Sci.*, 2021, **64**, 187–190.
- 25 H. Legros, J. Mercadier, J. Villeneuve, R. L. Romer, E. Deloule, M. V. Lichtervelde, S. Dewaele, P. Lach, X. D. Che, R. C. Wang, Z. Y. Zhu, E. Gloaguen and J. Melleton, *Chem. Geol.*, 2019, **512**, 69–84.
- 26 F. Melcher, M. A. Sitnikova, T. Graupner, N. Martin, T. Oberthür, F. Henjes-Kunst, H. E. Gäbler, A. Gerdes, H. Brätz, D. W. Davis and S. Dewaele, *SGA News*, 2008, vol. 23, pp. 1–14.
- 27 S. Dewaele, F. Henjes-Kunst, F. Melcher, M. Sitnikova, R. Burgess, A. Gerdes, M. A. Fernandez, F. De Clercq, F. Muchez and B. Lehmann, *J. Afr. Earth Sci.*, 2011, **61**, 10–26.
- 28 X. D. Deng, J. W. Li, X. F. Zhao, Z. C. Hu, H. Hu, D. Selby and Z. S. de Souza, *Chem. Geol.*, 2013, **344**, 1–11.
- 29 X. D. Che, F. Y. Wu, R. C. Wang, A. Gerdes, W. Q. Ji, Z. H. Zhao, J. H. Yang and Z. Y. Zhu, *Ore Geol. Rev.*, 2015, **65**, 979–989.
- 30 X. D. Che, R. C. Wang, F. Y. Wu, Z. Y. Zhu, W. L. Zhang, H. Hu, L. Xie, J. J. Lu and D. Zhang, *Ore Geol. Rev.*, 2019, **105**, 71–85.
- 31 M. Van Lichtervelde, A. Grand'Homme, M. de Saint-Blanquat, P. Olivier, A. Gerdes, J. L. Paquette, J. C. Melgarejo, E. Druguet and P. Alfonso, *Mineral. Petrol.*, 2017, **111**, 1–21.
- 32 F. Yuan, S. Y. Jiang, C. L. Wang, G. Jin, J. Zhang, H. X. Zhang and X. J. Hu, *Ore Geol. Rev.*, 2022, **140**, 104634.
- 33 J. Melleton, E. Gloaguen, D. Frei, M. Novák and K. Breiter, *Can. Mineral.*, 2012, **50**, 1751–1773.
- 34 L. Xiang, R. C. Wang, R. L. Romer, X. D. Che, H. Hu and Z. M. Tang, *Geostand. Geoanal. Res.*, 2023, DOI: [10.1111/ggr.12500](https://doi.org/10.1111/ggr.12500).
- 35 Z. Y. Yang, R. C. Wang, X. D. Che, L. Xie and H. Hu, *Am. Miner.*, 2022, **107**, 2155–2166.
- 36 Q. F. Zhou, K. Z. Qin and D. M. Tang, *J. Asian Earth Sci.*, 2021, **218**, 104879.
- 37 G. C. Fei, J. F. Menuge, Y. Q. Li, J. Y. Yang, Y. Deng, C. S. Chen, Y. F. Yang, Z. Yang, L. Y. Qin, L. Zheng and W. C. Tang, *Lithos*, 2020, **364–365**, 15555.
- 38 G. C. Fei, Z. Yang, J. Y. Yang, W. Luo, Y. Deng, Y. T. Lai, X. X. Tao, L. Zheng, W. C. Tang and J. Li, *Acta Geol. Sin.*, 2020, **94**, 836–849. In Chinese with English Abstract.
- 39 P. Li, J. K. Li, X. Liu, C. Li, Z. B. Huang and F. C. Zhou, *Ore Geol. Rev.*, 2020, **116**, 103237.
- 40 K. P. Jochum, U. Weis, B. Stoll, D. Kuzmin, Q. C. Yang, I. Raczek, D. E. Jacob, A. Stracke, K. Birbaum, D. A. Frick,

- D. Günther and J. Enzweiler, *Geostand. Geoanal. Res.*, 2011, **35**, 397–429.
- 41 Q. Ma, N. J. Evans, X. X. Ling, J. H. Yang, F. Y. Wu, Z. D. Zhao and Y. H. Yang, *Geostand. Geoanal. Res.*, 2019, **43**, 355–384.
- 42 M. Yang, Y. H. Yang, S. L. Kamo, R. L. Romer, N. M. W. Roberts, H. Wang, L. W. Xie, C. Huang, J. H. Yang and F. Y. Wu, *Geostand. Geoanal. Res.*, 2022, **46**, 169–203.
- 43 J. Hiess, D. J. Condon, N. Mclean and S. R. Noble, *Science*, 2012, **335**, 1610–1614.
- 44 S. T. Wu, G. Wörner, K. P. Jochum, B. Stoll, K. Simon and A. Kronz, *Geostand. Geoanal. Res.*, 2019, **43**, 567–584.
- 45 W. L. Griffin, W. J. Powell, N. J. Pearson and S. Y. O'Reilly, *Mineral. Assoc. Can., Short Course*, 2008, **40**, 308–311.
- 46 M. Yang, R. L. Romer, Y. H. Yang, S. T. Wu, H. Wang, J. R. Tu, H. Y. Zhou, L. W. Xie, C. Huang, L. Xu, J. H. Yang and F. Y. Wu, *Chem. Geol.*, 2022, **593**, 120754.
- 47 K. R. Ludwig, *Isoplot/Ex, Version 4.15: A geochronological toolkit for Microsoft Excel*, Berkeley Geochronol. Cent., Spec. Publ., no. 4, 2011.
- 48 J. S. Stacey and J. D. Kramers, *Earth Planet. Sci. Lett.*, 1975, **26**, 207–221.
- 49 X. Zeng, X. L. Mao and R. E. Greif, *Appl. Phys. A*, 2005, **80**, 237–241.
- 50 F. Poitrasson and F. X. d'Abzac, *J. Anal. At. Spectrom.*, 2017, **32**, 1075–1091.
- 51 C. O'Connor, B. L. Sharp and P. Evans, *J. Anal. At. Spectrom.*, 2006, **21**, 556–565.
- 52 M. Oeser, S. Weyer, I. Horn and S. Schuth, *Geostand. Geoanal. Res.*, 2014, **38**, 311–328.
- 53 T. Luo, Z. C. Hu, W. Zhang, Y. S. Liu and K. Q. Zong, *Anal. Chem.*, 2018, **90**, 9016–9024.
- 54 Y. Tang, J. Y. Zhao, H. Zhang, D. W. Cai, Z. H. Lv, Y. L. Liu and X. Zhang, *Ore Geol. Rev.*, 2017, **83**, 300–311.
- 55 Q. H. Yan, Z. W. Qiu, H. Wang, M. Wang, X. P. Wei, P. Li, R. Q. Zhang, C. Y. Li and J. P. Liu, *Ore Geol. Rev.*, 2018, **100**, 561–573.
- 56 A. H. Jaffey, K. F. Flynn, L. E. Glendenin, W. C. Bentley and A. M. Essling, *Phys. Rev. C: Nucl. Phys.*, 1971, **4**, 1889–1906.
- 57 D. M. Chew, J. A. Petrus and B. S. Kamber, *Chem. Geol.*, 2014, **365**, 185–199.